Draft version October 23, 2013
Preprint typeset using LaTeX style emulateapj v. 5/2/11

ON THE MINIMUM CORE MASS FOR GIANT PLANET FORMATION

Ana-Maria A. Piso
Harvard-Smithsonian Center for Astrophysics

Andrew N. Youdin
JILA, University of Colorado at Boulder
Draft version October 23, 2013

ABSTRACT

1. INTRODUCTION

Kelvin-Helmholz (KH) contraction considered previously (Ikoma, PapNel05). Say why useful. This paper develops a simplified model of KH contraction to both elucidate the relevant physical processes and explore a wide range of disk parameter space...

This paper is organized as follows. In Section 2 we describe the assumptions of our atmosphere model, and derive the basic equations that govern the structure and evolution of the atmosphere. In Section 3, we present a simplified analytic model that predicts the qualitative behavior of the numerical model. Results for atmospheric structure and evolution are presented in Section 4, and implications for the critical core mass are presented in Section 5. The discussion in Section 6 addresses various approximations and neglected effects. We summarize our findings in Section 7. The appendices contain...

2. ATMOSPHERE MODELS

To model the growth of planetary atmospheres around a solid core, we develop a simplified two layer model for time-dependent atmospheric cooling, i.e. Kelvin-Helmholtz (KH) contraction. With a convective interior and radiative exterior, this model is motivated by similar models of hot Jupiters (Arras & Bildsten 2006; Youdin & Mitchell 2010).

Our model can accurately model the growth of the atmosphere up to the crossover mass, when the atmosphere mass equals the mass of the core. Beyond the crossover mass, our approximate treatment of the radiative zone (explained below) breaks down. Since subsequent growth is a rapid runaway process (Pollack et al. 1996), our model can investigate to good accuracy the timescale requirement of core accretion. Our simplified treatment is also inappropriate for hot, short-period planets, where dust sublimation gives deeper radiative zones that require more detailed models.

Our main assumptions are summarized as follows:

1. The atmosphere is spherically symmetric and remains in hydrostatic balance during its thermal evolution.
2. The core mass and radius are fixed in evolutionary calculations, neglecting ongoing planetesimal or dust accretion.
3. At the planet's Hill radius, the atmospheric temperature and pressure match the conditions of the disk midplane.
4. The only source of planetary luminosity is the gravitational contraction of the atmosphere.
5. In the radiative zone, luminosity generation is neglected, i.e. the luminosity is held constant.
6. A global cooling model connects independent static solutions into a time-dependent sequence.
7. A polytropic EOS is assumed for simplicity.
8. Dust grains provide the opacity in the radiative zone, which remains cool enough to avoid dust sublimation.
9. Because gas accretion accelerates after the crossover mass, the time to reach the crossover mass is a good approximation of the total time to form a gas giant.

The remainder of this section develops our model in more detail.

2.1. *Disk and Opacity Model*

We adopt a minimum mass solar nebula (MMSN) model for a passively irradiated disk (Chiang & Youdin 2010). With the semi-major axis a normalized to the outer disk as $a_{10} = a/(10\text{ AU})$, the gas surface density and mid-plane temperature are

$$\Sigma_{\rm d} = 70\, F_\Sigma a_{10}^{-3/2}\ \text{g cm}^{-2} \tag{1a}$$

$$T_{\rm d} = 45\, F_T\, a_{10}^{-3/7}\ \text{K}\,. \tag{1b}$$

The normalization factors F_Σ and F_T adjust the model relative to the fiducial MMSN. We fix $F_\Sigma = F_T = 1$ unless noted otherwise.

For a vertically isothermal disk in hydrostatic balance (with no self-gravity), the mid-plane pressure of disk gas is

$$P_{\rm d} = 6.9\times 10^{-3} F_\Sigma \sqrt{F_T}\, a_{10}^{-45/14}\ \text{dyne cm}^2 \tag{2}$$

for a molecular weight of $\mu = 2.35$ proton masses and a Solar mass star.

The (thermodynamically isothermal) sound speed in the disk is

$$c_{\rm d} = \sqrt{\mathcal{R} T_{\rm d}} = 0.4\sqrt{F_T} a_{10}^{3/14}\ \text{km s}^{-1} \tag{3}$$

in terms of the specific gas constant $\mathcal{R}$. The disk scale-height is

$$H_{\rm d} = c_{\rm d}/\Omega = 0.42\sqrt{F_T}\, a_{10}^{9/7}\ \text{AU}\,. \tag{4}$$

in terms of the Keplerian frequency $\Omega = \sqrt{GM_*/a^3}$ with G the gravitational constant and M_* the stellar (in this work Solar) mass.

We assume a dust opacity following Bell & Lin (1994):

$$\kappa = 2F_\kappa \left(\frac{T}{100\ \mathrm{K}}\right)^\beta\ \mathrm{cm}^2\ \mathrm{g}^{-1}, \tag{5}$$

with a powerlaw index $\beta = 2$ and normalization $F_\kappa = 1$ unless noted otherwise. Grain growth tends to lower both F_κ and β, while dust abundance scales with F_κ. Section 6.2 discusses dust sublimation and more realistic opacity laws.

2.2. *Length Scales*

The characteristic length scales for protoplanetary atmospheres are crucial for choosing boundary conditions and for understanding the validity of spherical symmetry in a disk of scaleheight H_d. The radius of the solid core:

$$R_\mathrm{c} \equiv \left(\frac{3M_\mathrm{c}}{4\pi\rho_\mathrm{c}}\right)^{1/3} \approx 10^{-4} m_\mathrm{c10}^{1/3}\ \mathrm{AU}, \tag{6}$$

where the core mass, M_c, is normalized to 10 Earth masses as $m_\mathrm{c10} \equiv M_\mathrm{c}/(10\ M_\oplus)$. The core density is held fixed at $\rho_\mathrm{c} = 3.2\ \mathrm{g\ cm}^{-3}$. We thus neglect the detailed equation of state of the solid core (Fortney et al. 2007).

A planet can bind a dense atmosphere if the escape speed exceeds the sound speed. This criterion is satisfied inside the Bondi radius

$$R_\mathrm{B} \equiv \frac{GM_\mathrm{p}}{c_\mathrm{d}^2} \approx 0.17\,\frac{m_\mathrm{p10}\,a_{10}^{3/7}}{F_T}\ \ \mathrm{AU} \tag{7}$$

where the enclosed planet mass, $M_\mathrm{p} = M_\mathrm{c} + M_\mathrm{atm}$, includes the core and any atmosphere within the Bondi radius. The scalings thus use $m_\mathrm{p10} \equiv M_\mathrm{p}/(10\ M_\oplus)$.

Stellar tides dominate the planet's gravity beyond the Hill radius

$$R_\mathrm{H} = \left(\frac{M_\mathrm{p}}{3M_*}\right)^{1/3} a \approx 0.22\, m_\mathrm{p10}^{1/3}\, a_{10}\ \ \mathrm{AU} \tag{8}$$

where hydrostatic balance breaks down. In Equation (8), M_p includes mass enclosed within R_H. During the early stages of evolution, $M_\mathrm{p} \sim M_\mathrm{c}$, and the core mass can be used to get estimates of both R_B and R_H.

The relevant length scales of the atmosphere and disk satisfy the relation $R_\mathrm{B} H_\mathrm{d}^2 = 3R_\mathrm{H}^3$. The lengthscales are roughly equal at the "thermal mass"

$$M_\mathrm{th} > \frac{c_\mathrm{d}^3}{G\Omega} \approx 25\,\frac{F_T^{3/2}}{\sqrt{m_*}}\,a_{10}^{6/7}\ M_\oplus\,. \tag{9}$$

In the low mass regime, $M_\mathrm{p} < M_\mathrm{th}/\sqrt{3}$, the lengthscales order as $R_\mathrm{B} < R_\mathrm{H} < H_\mathrm{d}$ (R06). In this regime, many studies assume the atmosphere matches the disk conditions at R_B. We however use R_H as the matching radius in both this low mass and other higher mass regimes. This choice is justified by the fact that, for hydrostatic solutions, the density at R_B exceeds the disk's background density by an order unity factor (R06). This modest density change has a similarly modest effect on our results.

For a finite range of intermediate masses, $M_\mathrm{th}/\sqrt{3} < M_\mathrm{p} < 3M_\mathrm{th}$, the Hill radius is the smallest scale, satisfying both $R_\mathrm{H} < R_\mathrm{B}$ and $R_\mathrm{H} < H_\mathrm{d}$. Spherical symmetry remains a good, if imperfect, approximation because the disk is only weakly vertically stratified on scales $\lesssim H_\mathrm{d}$.

At higher planet masses where $M_\mathrm{p} > 3M_\mathrm{th}$ and $H_\mathrm{d} < R_\mathrm{H} < R_\mathrm{B}$, spherical symmetry is no longer a good approximation, due to both the vertical stratification of the disk and gap opening. See §6.1 for discussion of neglected non-hydrostatic effects on all mass scales.

Note that while R_H is the outer boundary of our structure calculations, we define planet masses to include only the mass inside the smaller of R_B or R_H. This conservative choice in quoting planet masses is usually a minor distinction because (when $R_\mathrm{B} < R_\mathrm{H}$) the gas between R_B and R_H is weakly compressed.

2.3. *Structure Equations and Boundary Conditions*

Our atmosphere calculations use the standard structure equations of mass conservation, hydrostatic balance, thermal gradients, and energy conservation:

$$\frac{dm}{dr} = 4\pi r^2 \rho \tag{10a}$$

$$\frac{dP}{dr} = -\frac{Gm}{r^2}\rho \tag{10b}$$

$$\frac{dT}{dr} = \nabla \frac{T}{P}\frac{dP}{dr} \tag{10c}$$

$$\frac{dL}{dr} = 4\pi r^2 \rho \left(\epsilon - T\frac{\partial S}{\partial t}\bigg|_m\right), \tag{10d}$$

where r is the radial coordinate, P, T, ρ and L are the gas pressure, temperature, density and luminosity, respectively. The enclosed mass at radius r is m. Equation (10c) simply defines the temperature gradient $\nabla \equiv d\ln T/d\ln P$. In radiative zones radiative diffusion gives a temperature gradient

$$\nabla_\mathrm{rad} \equiv \frac{3\kappa P}{64\pi G m \sigma T^4} L, \tag{11}$$

where σ is the Stefan-Boltzmann constant. In convectively unstable regions, efficient convection gives an isentropic temperature gradient with $\nabla = \nabla_\mathrm{ad}$, the adiabatic gradient (i.e. the temperature gradient at constant entropy). According to the Schwarzschild criterion, convective instability occurs when $\nabla_\mathrm{rad} > \nabla_\mathrm{ad}$. Thus $\nabla = \min(\nabla_\mathrm{rad}, \nabla_\mathrm{ad})$ sets the temperature gradient.

In the energy equation (10d), ϵ represents all local sources of heat input, which excludes the motion of the atmosphere itself. In stars, nuclear burning contributes to ϵ. In a protoplanetary atmosphere, dissipative drag on planetesimals contributes to ϵ. Our simplified models set $\epsilon = 0$, consistent with our neglect of planetesimal accretion luminosity at the base of the atmosphere. The $\epsilon_\mathrm{g} = -T\partial S/\partial t$ term gives the energy input from gravitational contraction.[1] The partial time derivative would normally require our radial derivatives to be partial derivatives. However our subsequent developments will replace the local energy equation (10d)

[1] In general, any motion in a non-stationary atmosphere is accounted for by this term. The partial time derivative is performed on shells of fixed mass.

with global energy balance, reverting the structure equations to time-independent ordinary differential equations (ODEs).

To solve the equation set (10) an equation of state (EOS) is required for closure. In our study, we adopt an ideal gas law with a polytropic EOS

$$P = \rho \mathcal{R} T \,, \tag{12a}$$
$$P = K \rho^{\gamma} \,, \tag{12b}$$

where K is the adiabatic constant. The adiabatic index $\gamma = 1/(1-\nabla_{\rm ad})$. An ideal monatomic gas has $\nabla_{\rm ad} = 2/5$. This work uses $\nabla_{\rm ad} = 2/7$ for an ideal diatomic gas. While our reference mean molecular weight ($\mu = 2.35$ proton masses) includes Helium, we ignore Helium's effect on the EOS, which is already greatly simplified. The second law or thermodynamics gives the relative entropy as

$$S = \mathcal{R} \ln \left(\frac{T^{1/\nabla_{\rm ad}}}{P} \right) \tag{13}$$

eliminating the need for K.

Boundary conditions must be satisfied at both the base and the top of the atmosphere with $m(R_{\rm c}) = M_{\rm c}$, $T(R_{\rm H}) = T_{\rm d}$ and $P(R_{\rm H}) = P_{\rm d}$. In principle our solutions describe atmospheres with $L(R_{\rm c}) = 0$. In practice, since we do not directly integrate Equation (10d) we need not directly impose this boundary condition, as described in §2.5.

2.4. *Global Cooling of an Embedded Planet*

This section describes the global energy balance of a planet embedded in a gas disk, or more generally any spherical, hydrostatic object in pressure equilibrium with a background medium. The total atmospheric energy includes gravitational and internal energies, $E = E_G + U$:

$$E_G = -\int_{M_{\rm c}}^{M} \frac{Gm}{r} dm \,, \tag{14a}$$
$$U = \int_{M_{\rm c}}^{M} u dm \,. \tag{14b}$$

The specific internal energy $u = C_V T = \mathcal{R}(\nabla_{\rm ad}^{-1} - 1)T$ for a polytropic EOS. For a star or coreless planet, $L_{\rm c} = M_{\rm c} = 0$.

We start with the global energy balance for an isolated planet with a free surface:

$$L_M = L_{\rm c} + \Gamma - \dot{E}. \tag{15}$$

The surface luminosity, L_M, includes contributions from the core luminosity $L_{\rm c}$ – e.g. planetesimal accretion or radioactive decay – from the total heat generation Γ – given by the integral of ϵ over the object – and from the rate of change of atmospheric energy $\dot{E}$, a loss term.

For an object with no core luminosity (or no core) and no internal heat sources, the energy equation $L_M = -\dot{E}$ describes KH contraction in its simplest form. For a main sequence star $L_M = \Gamma$ as the heat of nuclear burning supplies the total luminosity.

For a protoplanetary atmosphere embedded in a gas disk, the full energy equation,

$$L_M = L_{\rm c} + \Gamma - \dot{E} + e_M \dot{M} - P_M \left. \frac{\partial V_M}{\partial t} \right|_M \,, \tag{16}$$

acquires surface terms as derived in Appendix A. The energy accreted across the surface is given by the specific energy, $e_M = u_M - GM/R$, and the mass accretion rate of gas, $\dot{M}$. The work done by the surface is $P_M \partial V_M / \partial t$, with the partial derivative performed at fixed mass. This generalized energy equation applies on any spherical shell where hydrostatic balance holds.[2] Thus M no longer refers to a uniquely defined total mass, but to the chosen mass level, where the instantaneous radius is R. Values on this shell are labelled by M subscripts.

For static solutions, which are not the focus of this Paper, the surface terms (and also $\dot{E}$) vanish. Static solutions are valid when imposed heat sources, i.e. $L_{\rm c}$ and Γ exceed the atmospheric losses. Quantitatively, static solutions apply when the evolutionary timescale exceeds the KH timescale,

$$\tau_{\rm KH} \sim \frac{|E|}{L_M}, \tag{17}$$

where surface terms are assumed to be subdominant. Thus evolutionary calculations, including the quasistatic calculations of this Paper, are needed to consider the fastest possible evolution that occurs on $\tau_{\rm KH}$.

2.5. *The Two-Layer Model*

To simplify our calculations of atmospheric contraction we use a two layer model with a bottom convective region and an upper radiative layer. The existence of such a structure is well known from previous studies (R06) and can be readily understood. Before the protoplanetary atmosphere can cool, it has the entropy of the disk. As the atmosphere cools the deep interior remains convective. Convective interiors are a common feature of low mass cool objects (brown dwarfs and planets) that results from the behavior of $\nabla_{\rm rad}$ for realistic opacity laws. However the entropy of the deep interior decreases as the atmosphere cools. A region of outwardly increasing entropy, i.e. a radiative layer, is required to connect the convective interior to the disk. A more complicated structure, with radiative windows in the convection zone, is possible as discussed in §6.2.

In convective regions, the adiabatic structure is independent of luminosity and can be calculated without local energy balance, Equation (10d). Thus for fully convective objects, a cooling sequence can be established by connecting a series of adiabatic solutions using a global energy equation, $L_M = -\dot{E}$ or Equation (15). Such methods are commonly used for their computational efficiency and are sometime referred to as "following the adiabats," since the steady state solutions evolve in order of decreasing entropy (Marleau & Cumming 2013).

In the radiative zone, local energy balance, Equation (10d), does affect the atmospheric structure. We proceed by assuming that the majority of energy is lost from the convective interior, and thus the luminosity can be treated as constant in the outer radiative zone. With this approximation we can construct solutions from equa-

[2] Equation (16) also applies in the interior of objects with a free surface. The work term, $P_M \partial V_M / \partial t$, vanishes at the free surface. The accretion energy, $e_M \dot{M}$, vanishes for a truly isolated object, but would be included to account for accretion onto (or mass loss from) an otherwise free surface.

tions (10a – c) that "follow the mass," i.e. gradually increase the atmospheric mass. We then use the global energy balance, Equation (16) to connect these solution in a cooling sequence. The validity of neglecting luminosity generation in the radiative zone can be checked *a posteriori*.

To make a single atmosphere model (indexed by i) we choose a planet mass M_i. At the outer boundary, at $R_{\rm H}(M_i)$, the temperature and pressure are set to the disk values. To integrate equations (10a–c), the luminosity is required to compute $\nabla_{\rm rad}$. The correct value of the luminosity is the eigenvalue of the problem, which we find by the shooting method. Only for the eigenvalue of luminosity does the integrated value of mass at the core, $m(R_{\rm c})$, match the actual core mass, $M_{\rm c}$.

To establish the time difference between neighboring solutions, we apply Equation (16) at the radiative-convective boundary (RCB) of the solutions. Using exact solutions, energy balance could be evaluated at any level. The approximation of constant luminosity in the radiative zone makes the RCB the self-consistent choice. After setting $\Gamma = L_{\rm c} = 0$, we solve for the elapsed time Δt between states i and $i+1$ by finite differencing to give

$$\Delta t = \frac{-\Delta E + \langle e \rangle \Delta M - \langle P \rangle \Delta V_{\langle M \rangle}}{\langle L \rangle} \,. \tag{18}$$

Brackets indicate an average of, and Delta (Δ) indicates a difference between, neighboring solutions. All values are evaluated at the RCB. Due to the partial derivative in Equation (16), the volume difference $\Delta V_{<M>}$ is performed at fixed mass, here the average of the masses at the RCB.

3. ANALYTIC COOLING MODEL

This section develops the analytic version of our two-layer model, which is useful for predicting and explaining the results of numerical evolution models. To obtain our analytic results, we neglect self-gravity. As shown in Section 4, self-gravity becomes quantitatively important at surprisingly low atmospheric masses, $M_{\rm atm} \gtrsim 0.2 M_{\rm c}$. Thus the analytic model cannot accurately model the the later stages of evolution. Nevertheless, the analytic model does successfully explain general trends with e.g. opacity and disk temperature and pressure.

The analytic model also assumes that the upper radiative radiative layer is thick, with a pressure depth $P_{\rm RCB} \gg P_{\rm d}$. This approximation limits the ability to study the initial cooling of very low mass atmospheres. However since early evolution is quite rapid, this approximation negligibly affects total cooling times and criticial core masses, our main foci.

3.1. *Two Layer Structure*

To apply the two layer cooling model analytically, we require expressions for the atmospheric structure. Conditions at the RCB are crucial as they set the interior adiabat and the radiative losses. (Recall that luminosity generation in the radiative zone is neglected.) We express the temperature and pressure of the RCB, at the radius $R_{\rm RCB}$, as

$$T_{\rm RCB} = \chi T_{\rm d} \tag{19a}$$

$$P_{\rm RCB} = \theta P_{\rm d} e^{R_{\rm B}/R_{\rm RCB}} \,. \tag{19b}$$

If the radiative zone were replaced by an isothermal layer, then hydrostatic balance would give $\chi = \theta = 1$. Standard radiative structure calculations (see Appendix B for details) give

$$\chi \simeq \left(1 - \frac{\nabla_{\rm ad}}{\nabla_\infty}\right)^{-\frac{1}{4-\beta}} \simeq 1.53 \,, \tag{20}$$

for $P_{\rm RCB} \gg P_{\rm d}$, our regime of interest, and with the radiative temperature gradient at infinite depth, $\nabla_\infty = 1/2$, for our dust opacity. The radiative zones are thus nearly isothermal, as also found by R06. While a simple closed form expression is not possible, the factor $\theta \simeq 0.556$ for our parameters. According to Equation (19b) our pressure criterion also gives $R_{\rm RCB} \ll R_{\rm B}$, but the inequality is logarithmically weaker.

Given the conditions at the RCB, hydrostatic balance gives the density and temperature profiles along the adiabat,

$$\rho = \rho_{\rm RCB} \left[1 + \frac{R'_{\rm B}}{r} - \frac{R'_{\rm B}}{R_{\rm RCB}}\right]^{1/(\gamma-1)} \tag{21a}$$

$$T = T_{\rm RCB} \left[1 + \frac{R'_{\rm B}}{r} - \frac{R'_{\rm B}}{R_{\rm RCB}}\right] . \tag{21b}$$

The effective Bondi radius

$$R'_{\rm B} \equiv \frac{G M_{\rm c}}{C_P T_{\rm RCB}} = \frac{\nabla_{\rm ad}}{\chi} R_{\rm B} \tag{22}$$

simplifies expressions, with $C_P = \mathcal{R}/\nabla_{\rm ad}$ the specific heat at constant pressure.

Even simpler expressions hold deep in the adiabatic interior, where $r \ll R_{\rm RCB} \ll R'_{\rm B}$ gives

$$\rho \simeq \rho_{\rm RCB} \left[\frac{R'_{\rm B}}{r}\right]^{1/(\gamma-1)} \propto r^{-5/2} \tag{23a}$$

$$T \simeq T_{\rm RCB} \frac{R'_{\rm B}}{r} = \frac{G M_{\rm c}}{C_P r} \,. \tag{23b}$$

While the radial density profile depends on the adiabatic index, the temperature scaling does not. For reference, if self-gravity is included, the temperature profile satifies

$$\frac{dT}{dr} = -\frac{G m(r)}{C_P r^2} \,. \tag{24}$$

Thus the enclosed mass in self-gravitating models gives a temperature profile flatter than $T \propto r^{-1}$.

The total specific energy at depth

$$e = e_g + u = -\nabla_{\rm ad} \frac{G M_{\rm c}}{r} \,. \tag{25}$$

is thus generically proportional to the gravitational potential, $e_G = -G M_{\rm c}/r$.

3.2. *Mass, Energy and Luminosity*

The most relevant quantities for the global cooling model are the integrated energy, luminosity, and atmospheric mass. In our non-self-gravitating limit, the mass of our nearly isothermal radiative zones is less than the convective interior, as shown in Appendix B.

Equation (21a) thus integrates to give the atmospheric mass

$$M_{\rm atm} = \frac{5\pi^2}{4} \rho_{\rm RCB} {R'_{\rm B}}^{5/2} \sqrt{R_{\rm RCB}}, \tag{26}$$

in the relevant limit $R_{\rm c} \ll R_{\rm RCB} \ll R'_{\rm B}$ and for $\gamma = 7/5$. Mass is concentrated near the outer regions of the convective zone, a result that holds more generally for $\gamma > 4/3$.

Using Equation (19b) to eliminate $R_{\rm RCB}$, the critical ratio of atmosphere to core mass becomes

$$\frac{M_{\rm atm}}{M_{\rm c}} = \frac{P_{\rm RCB}}{\xi P_M}, \tag{27}$$

where we define a characteristic pressure and a logarithmic factor

$$P_M \equiv \frac{4\nabla_{\rm ad}^{3/2}}{5\pi^2\sqrt{\chi}} \frac{GM_{\rm c}^2}{{R'_{\rm B}}^4} \tag{28a}$$

$$\xi \equiv \sqrt{\ln[P_{\rm RCB}/(\theta P_{\rm d})]}\,. \tag{28b}$$

The atmosphere mass increases as radiative losses lower the internal adiabat and increase $P_{\rm RCB}$. The crossover mass, $M_{\rm atm} = M_{\rm c}$, is reached when

$$P_{\rm RCB} = \xi P_M, \tag{29}$$

i.e. near the characteristic pressure P_M. The critical value of the order unity factor ξ is found by eliminating $P_{\rm RCB}$ from Equations (28b) and (29). This logarithmic factor complicates our analytic description, but since it remains order unity we simply hold it fixed in our scalings.

The total energy is concentrated towards the core if $u\rho r^3 \propto \rho r^2$ drops with increasing r. This condition requires $\gamma < 3/2$, which our choice of $\gamma = 7/5$ satisfies, but $\gamma = 5/3$ does not. Integration of Equation (25) over the mass of the atmosphere thus gives

$$E = -4\pi\nabla_{\rm ad} G M_{\rm c} \int_{R_{\rm c}}^{R_{\rm RCB}} \rho r dr \tag{30a}$$

$$\approx -4\pi P_{\rm RCB} {R'_{\rm B}}^{\frac{1}{\nabla_{\rm ad}}} \left(\frac{\gamma-1}{3-2\gamma}\right) R_{\rm c}^{\frac{2\gamma-3}{\gamma-1}} \tag{30b}$$

$$\approx -8\pi P_{\rm RCB} \frac{{R'_{\rm B}}^{7/2}}{\sqrt{R_{\rm c}}} \tag{30c}$$

with $\gamma < 3/2$ and $\gamma = 7/5$ in Equations (30b) and (30c), respectively.

Applying marginal convective stability, $\nabla_{\rm rad} = \nabla_{\rm ad}$, to Equation (11) gives the emergent luminosity from the radiative-convective boundary,

$$L_{\rm RCB} = \frac{64\pi G M_{\rm RCB}\sigma T_{\rm RCB}^4}{3\kappa P_{\rm RCB}} \nabla_{\rm ad} \approx L_{\rm d} \frac{P_{\rm d}}{P_{\rm RCB}}\,, \tag{31}$$

where we define

$$L_{\rm d} \equiv \frac{64\pi G M_{\rm RCB}\sigma T_{\rm d}^4}{3\kappa(T_{\rm d}) P_{\rm d}} \nabla_{\rm ad} \chi^{4-\beta}. \tag{32}$$

The inverse scaling $L_{\rm RCB} \propto 1/P_{\rm RCB}$ shows that luminosity drops as the atmosphere cools and $P_{\rm RCB}$ deepens. This result relies on the pressure independence of dust opacities. For fully non-self-gravitating results, we replace $M_{\rm RCB}$, the mass up to the RCB, with the core mass, but the mass of the convective atmosphere could be included for a slightly higher order estimate.

3.3. *Simplified Cooling Model*

Our analytic cooling model uses $L = -\dot{E}$, neglecting the surface terms in Equation (16).[3] Applying Equations (30c) and (31) the time it takes to cool the atmosphere until the RCB reaches a given pressure depth, $P_{\rm RCB}$, is

$$t_{\rm cool} = -\int_{P_{\rm d}}^{P_{\rm RCB}} \frac{dE/dP_{\rm RCB}}{L} dP_{\rm RCB} \tag{33a}$$

$$\approx 4\pi \frac{P_{\rm RCB}^2}{P_{\rm d}} \frac{{R'_{\rm B}}^{7/2}}{L_{\rm d}\sqrt{R_{\rm c}}}\,. \tag{33b}$$

The initial RCB depth, set to $P_{\rm d}$ as a formality, is of little importance because the cooling slows it proceeds with $t_{\rm cool} \propto P_{\rm RCB}^2$.

The most relevant cooling time is the crossover time, $t_{\rm co}$, required to reach the crossover mass, $M_{\rm atm} = M_{\rm c}$. Equations (33) and (29) give this time as

$$t_{\rm co} \approx 2\times 10^8 \frac{F_T^{5/2} F_\kappa \left(\frac{\xi}{3.4}\right)^2}{m_{\rm c10}^{5/3} a_{10}^{15/14}} \text{ yr}\,. \tag{34}$$

The corresponding critical core mass, $M_{\rm crit}$, has a crossover time that equals the typical lifetime of a protoplanetary disk

$$t_{\rm d} = 3\times 10^6 \text{ yr}\,. \tag{35}$$

Setting $t_{\rm co} = t_{\rm d}$ gives

$$M_{\rm crit} \approx 100 \frac{F_T^{3/2} F_\kappa^{3/5} \left(\frac{\xi}{2.6}\right)^{6/5}}{a_{10}^{9/14}}\, M_\oplus. \tag{36}$$

Both $t_{\rm co}$ and $M_{\rm crit}$ are too large to be interesting, or to be correct based on previous results and the numerical results in this Paper. The main reason for this discrepancy is the neglect of self-gravity, as shown in Section 4. The magnitude of the discrepancy may be surprising as one might expect self-gravity to be a modest factor for $M_{\rm atm} \leq M_{\rm c}$. Clearly this seemingly reasonable expectation must be applied with caution, an interesting result in itself.

The analytic model is also useful because, despite the amplitude error, it explains the basic scaling of our (and other) numerical models. As is well known, a lower opacity, here scaling with F_κ, accelerates growth and gives a lower critical core mass. Lower disk temperatures also decrease both $t_{\rm co}$ and $M_{\rm crit}$. Furthermore the decline in both quantities with semimajor axis is completely generated by the disk temperature law (ignoring ξ). The temperature dependence are a competition between two main effects. The higher luminosity, $\propto T^{4-\beta}$, at higher temperatures gives faster cooling, which opposes the overall effect. The larger Bondi radius, and the effectively stronger gravity of the core, is the dominant effect that gives faster cooling at lower temperatures. For different β values, $t_{\rm co} \propto F_T^{\beta+1/2}$, so the slope of the dust opacity is an important moderating effect on the cooling.

[3] Appendix B shows that these terms are negligible for a non-self-gravitating model, but they do become relevant when self-gravity is important and included.

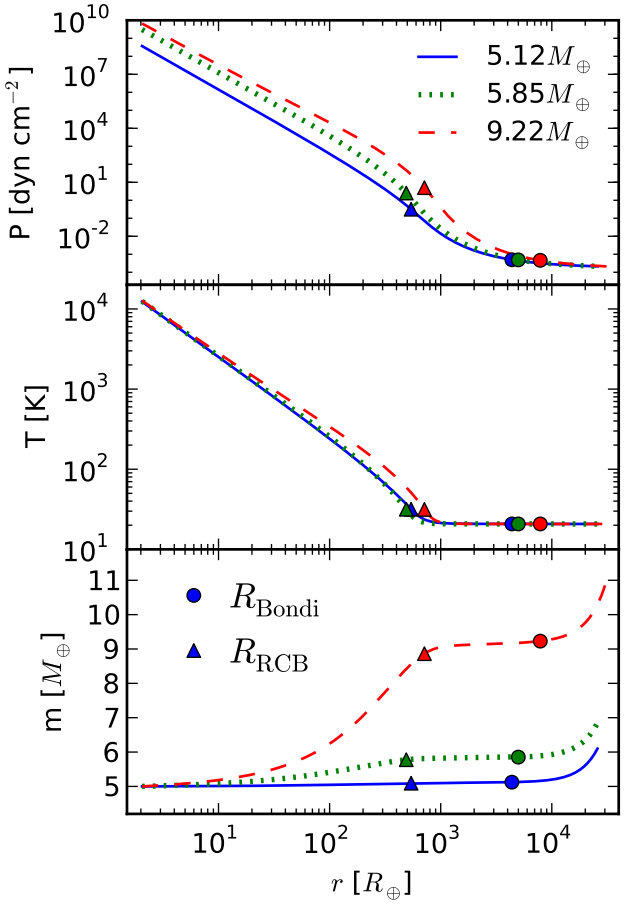

FIG. 1.— Radial profiles of atmospheric pressure, temperature and enclosed mass (including the core) for a $5M_\oplus$ core at $a = 60$ AU. Solid, dotted and dashed lines correspond to solutions with total mass (core and atmosphere) of $5.12M_\oplus$, $5.85M_\oplus$ and $9.22M_\oplus$, respectively. (See text for a description of evolution to yet higher masses.) Circles and triangles mark the locations of the Bondi radii and of the radiative-convective boundaries, respectively. The radial profiles extend from the core to the Hill radius.

The cooling timescale and critical core mass depend only weakly on the disk pressure, via the logarithmic factor ξ. Section 5.1.2 shows that these analytic predictions for disk temperature and pressure dependence compare favorably with numerical results.

TODO: consider adding "revised" analytic expressions for $t_{\rm co}$ and $M_{\rm crit}$ (e.g. lower Matm criterion). People like scalings, but the obviously wrong amplitudes will prevent people from using them unless we correct.

4. QUASI-STATIC KELVIN-HELMHOLTZ CONTRACTION

We now present some representative examples of the structure and evolution of our model atmospheres, calculated as described in §2, with some comparisons made to the non-self-gravitating analytic model of §3. Radial structure is presented in §4.1, time evolution is described in §4.2 and the regimes of validity of our two-layer cooling model are examined in §4.3.

4.1. *Atmospheric Stucture*

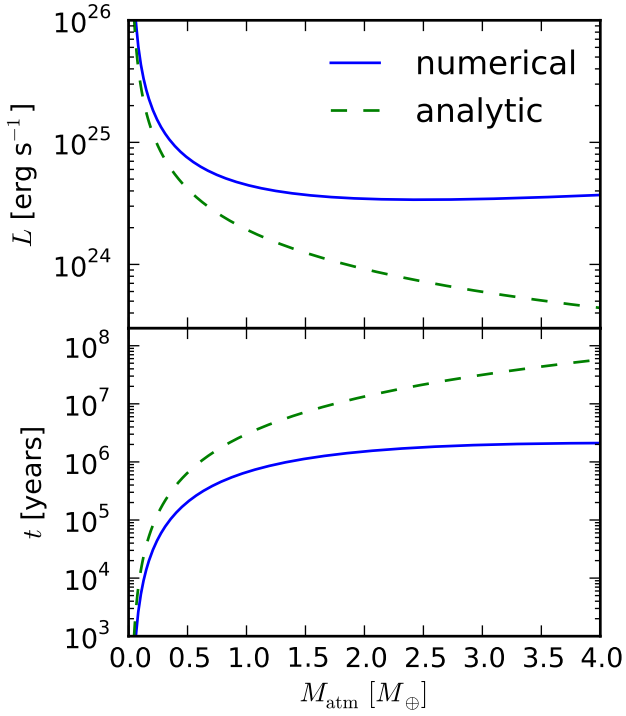

FIG. 2.— Evolution of the luminosity and elapsed time during atmospheric growth around a $5M_\oplus$ core at 60 AU. The luminosity is initially high, then decreases as the atmosphere grows in mass and the radiative zone becomes optically thicker. Due to the neglect of self-gravity, the analytic model (*dashed curve*) gives a further drop in luminosity and a longer evolution time.

Figure 1 shows radial profiles at different stages of atmospheric growth. In these examples, we fix the core mass at $M_{\rm c} = 5M_\oplus$ and the radial disk location to $a = 60$ AU. The quoted mass values include the core plus atmosphere within the smaller of $R_{\rm B}$ or $R_{\rm H}$, which for these cases is $R_{\rm B}$. The 9.22 $M_\oplus$ solution is the highest mass we can reach in our evolutionary sequence, as we explain further in §4.3.

Deep in a non-self-gravitating atmosphere, Equation (23) shows that $T \propto r^{-1}$ and $P \propto r^{-1/\nabla_{\rm ad}}$. This behavior is seen in the low mass solutions in Fig. 1. As explained by Equation (24), the higher mass solutions show a flatter profile in T and also in $P \propto T^{1/\nabla_{\rm ad}}$. In agreement with Equation (19), the radiative zone remains nearly isothermal – even in the more massive solutions – and thus shows a nearly exponential increase in pressure with inverse depth.

The higher mass atmosphere solutions have lower entropy, i.e. cooling allows the atmosphere to accrete more gas. This is evident in Fig. 1 from the higher internal pressures of the higher mass solutions. The somewhat higher temperatures in the higher mass solutions do not cause the entropy to increase.

4.2. *Time Evolution*

The cooling model of §2.5 is used to connect solutions of different atmospheric masses into an evolutionary sequence. Fig. 2 shows the luminosity evolution and the elapsed time as a function of atmospheric mass for a $5M_\oplus$ core at 60 AU, i.e. the same parameters as in Fig. 1. Dur-

ing the early stages of atmospheric growth, the luminosity drops sharply. This behavior is seen in both the full numerical solutions (with solid lines) and the analytic model (with dashed lines). As seen in Equation (31), the increased pressure depth of the RCB increases the optical depth ($\propto \kappa P$) and decreases the radiative luminosity.

At later stages of evolution, the numerical model gives a flat luminosity with increasing mass and also time (not shown). By contrast the analytic model gives a luminosity that continues to drop with increasing mass. The difference is due to the neglect of self-gravity in the analytic model. From Equation (31), $L_{\rm RCB} \propto M_{\rm RCB} T_{\rm RCB}^4/(\kappa_{\rm RCB} P_{\rm RCB})$. Thus accounting for the higher enclosed mass gives a somewhat higher luminosity in the self-gravitating model. However the main effect is the higher temperature in the self-gravitating models. The flatter temperature profiles with radius, as described above, explain why the self-gravitating models are hotter.

Fig. 3 shows the effect of decreasing the atmospheric dust abundance on the atmospheric evolution. The opacity normalization in Equation (5) is reduced by factors of 10 and 100. Lower opacities result in higher luminosities and faster evolution, a well-established result (Hubickyj et al. 2005) that we confirm for our model. Atmospheric dust opacities are difficult to robustly predict. Ablation of infalling solids is a dust source, while settling through the radiative zone is a sink. Grain growth both reduces dust opacities per unit mass and favors settling. Our scenario of negligible ongoing particle accretion tends to favor low dust opacities. To be conservative, however, our reference case considers full Solar abundances, but faster evolution is clearly possible.

Fig. 4 plots the evolution of the atmospheric growth timescale, $M_{\rm atm}/\dot{M}$, around a $5M_\oplus$ core at several locations in the disk. This instantaneous growth time shows clearly that the atmosphere spends the bulk of its time growing though intermediate atmospheric masses, $\sim 1{-}3$ $M_\oplus$ in this case. Growth times are short both early – when the radiative zone is relatively transparent – and late – when self-gravity accelerates growth. The accelerated growth at higher masses is also evident in Figs. 2 and 3 (bottom panels) as the flattening of the t vs. $M_{\rm atm}$ curve.

The fact that growth times peak before the crossover mass, when $M_{\rm atm} < M_{\rm c}$, is very helpful for understanding atmospheric growth. The estimated timescale to runaway growth can be well approximated by only considering the time it takes to grow to the crossover mass, or even to a somewhat lower mass. This insensitivity to the upper mass threshold is characteristic of accelerating growth, and is fortuitious. We next show how our model assumptions can break down during the later stages of atmospheric growth.

4.3. *Validity of the Two-Layer Cooling Model*

To examine the regimes where our cooling model is valid, we compare the model luminosity to the additional neglected luminosity, $L_{\rm negl}$, that a more detailed model would have generated in the radiative zone. To compute $L_{\rm negl}$ we compute the entropy difference between successive radiative zone solutions. We then integrate the energy equation, $\partial L/\partial m = -T\partial S/\partial t$, over the average

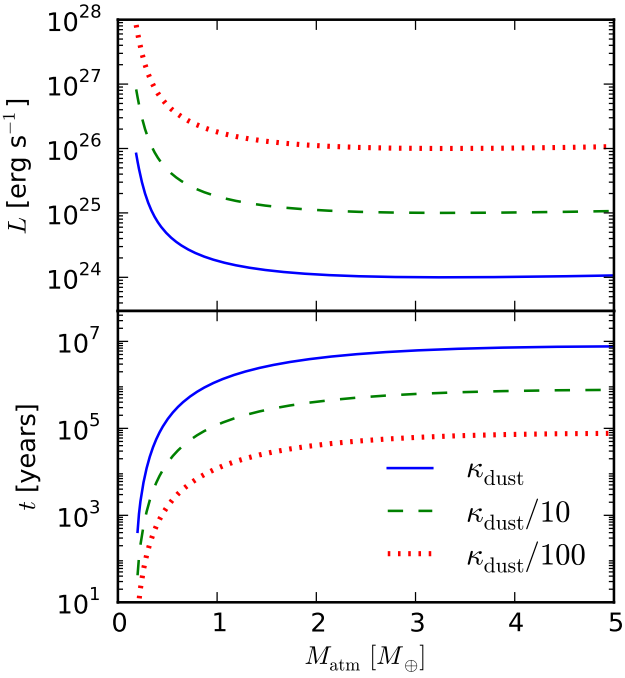

FIG. 3.— Similar to Fig. 2, but showing the effect of reducing the dust abundance by factors of 10 and 100 from standard Solar abundances. The reduced dust opacities give higher luminosities and faster atmospheric growth.

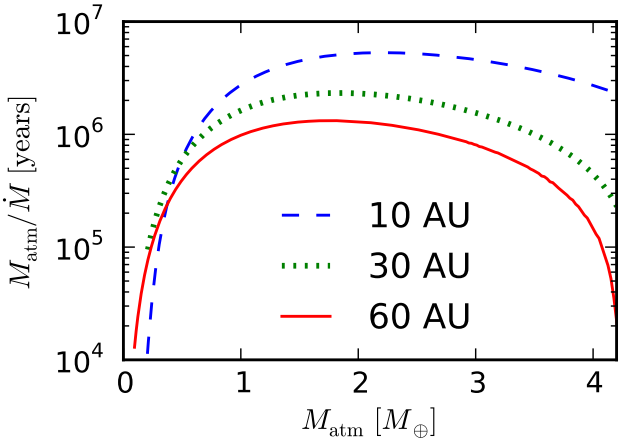

FIG. 4.— Evolution of the atmospheric growth timescale with mass around a $5M_\oplus$ solid core located at 10, 30 or 60 AU. Growth is slowest for $M_{\rm atm} \sim 1 - 3M_\oplus$, i.e. before the crossover mass at $M_{\rm atm} = M_{\rm c}$.

depth of the radiative zone.[4]

Fig. 4.3 shows that the neglected luminosity is indeed negligible during the early stages of evolution. However, $L_{\rm negl}$ exceeds the model luminosity, L, at high masses, $M_{\rm atm} > 3M_\oplus$ in this case, meaning that our model is becoming inaccurate. Nevertheless, our cooling model

[4] While useful as a diagnostic, the neglected luminosity cannot reliably correct the global cooling model because where $L_{\rm negl}$ is significant, the structure of the radiative zone would be inaccurate.

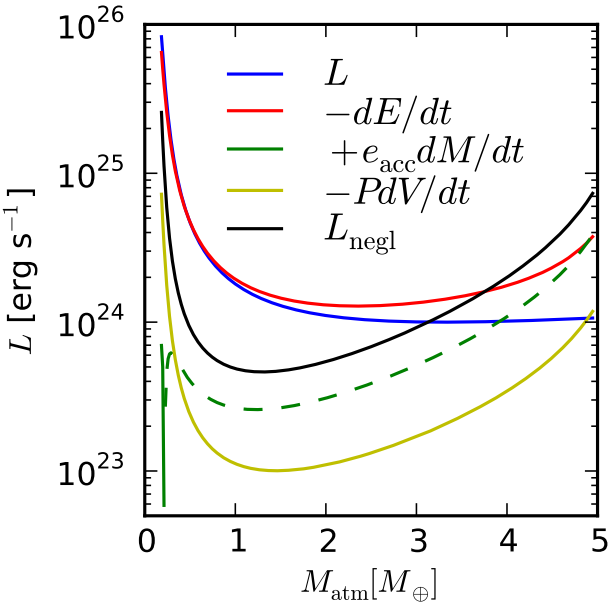

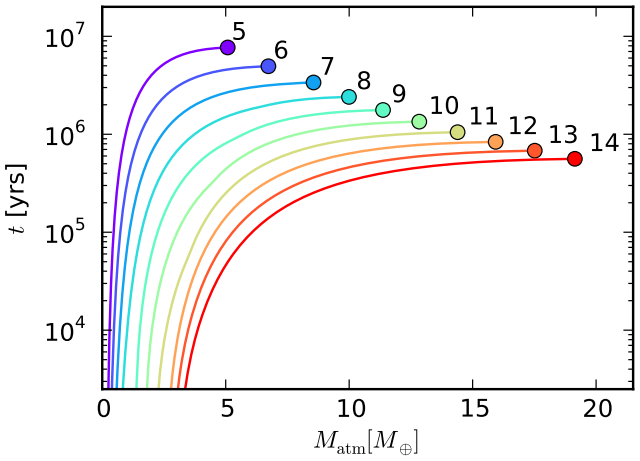

FIG. 5.— Time to grow an atmosphere of mass $M_{\rm atm}$ for cores with fixed masses between $5M_\oplus$ and $14M_\oplus$ (as labelled) at 10 AU in our fiducial disk. Circles mark the runaway growth time, $t_{\rm run}$, which occurs at roughly the crossover mass, $M_{\rm atm} = M_{\rm c}$. Larger core masses give faster atmospheric growth, to a fixed atmosphere mass and also to runaway. However, for larger $M_{\rm c}$, runaway growth commences at higher $M_{\rm atm}/M_{\rm c}$ values.

gives both conservative and reasonably reliable estimates of core accretion timescales. Our results are conservative – in the sense of overestimating growth times – because the neglected luminosity would give more rapid evolution. Moreover our results are reasonably accurate because the bulk of growth time is spent at low masses, when $L_{\rm negl}$ is small and safely neglected.

The (non-vanishing) individual terms in the global cooling model of Equation (16), evaluated at the RCB, are also plotted in Fig. 4.3. At low masses, the change in energy, $-\dot{E}$, makes the dominant contribution to luminosity. As the mass increases the surface terms become more significant, led by the accretion energy. However the surface terms are everywhere smaller than $L_{\rm negl}$. Thus while the surface terms appear to reduce the total luminosity (compared to $-\dot{E}$), $L_{\rm negl}$ can more than compensate, showing again that our model conservatively underestimates cooling.

At yet higher masses than shown in Fig. 4.3, our cooling model breaks down. Mathematically, the breakdown manifests as negative timesteps when advancing to a higher atmospheric mass. This unphysical result has no deep significance, as we already know that the neglected luminosity is large enough to give incorrect results. Sometimes this breakdown occurs even before the crossover mass is reached. The main practical effect of this behavior is that we halt the evolution where the model breaks down whenever we cannot reach the crossover mass. Fortunately the elapsed time to either the crossover mass or the breakdown is well-behaved and, most importantly, dominated by lower atmospheric masses where the model is accurate.

5. RESULTS FOR GIANT PLANET FORMATION

We now use our structure and evolution models to calculate the necessary conditions for gas giant formation by core accretion. Adopting a median disk lifetime of 3 Myr, we examine the conditions for a fixed mass core to to undergo runaway gas accretion within the lifetime of the gas disk. Our results for atmosphere growth times – for a range of core masses and disk conditions – are presented in §5.1. Section 5.2 gives our results for critical core masses, the minimum masses which can accrete a massive atmosphere within the disk lifetime.

Our models will focus on giant planet formation between 5 and 100 AU. The outer disk is of particular interest for direct imaging searches. The growth of atmospheres close to the star is also important, but spherical accretion models (including ours) are less applicable here. In the inner disk, critical core masses increase, yet lower mass planets start to open gaps and outgrow the disk scale height, see Equation (9). These concerns prevent us from applying our model to the inner disk.

5.1. *Runaway Growth Time Scale*

The time to undergo runaway growth of the atmosphere, $t_{\rm run}$, sets a minimum timescale for the formation of giant planets. Due to the accelerating nature of runaway growth, the precise threshold chosen for $t_{\rm run}$ (explained in §?) is of minor significance.

5.1.1. *Effects of Core Mass*

Fig. 5 demonstrates the growth of atmospheric mass with time for several core masses at 10 AU in our fiducial disk. Atmospheres grow faster around more massive cores due to stronger gravitational binding. The endpoint of each curve marks $t_{\rm run}$. Runaway growth occurs near the crossover mass, when $M_{\rm atm} \sim M_{\rm co}$ in agreement with previous studies. At lower core masses, however, runaway occurs at lower $M_{\rm atm}/M_{\rm c}$ ratios. Thus, when compared to the naive assumption that runaway occurs at a universal $M_{\rm atm}/M_{\rm c}$ ratio, effects that lower the critical core mass are amplified by the earlier onset of runaway growth.

Fig. 6 shows how $t_{\rm run}$ varies with core mass, also at 10 AU. The numerical results are plotted against our non-

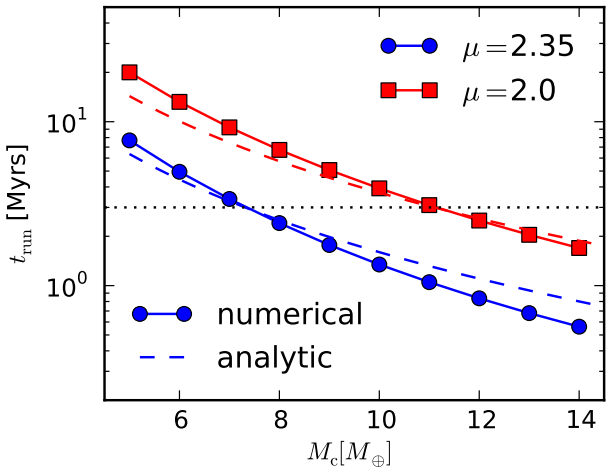

FIG. 6.— Runaway growth times, $t_{\rm run}$, vs. core mass at 10 AU, for two values of mean molecular weight. Our numerical model (*solid curves*) is compared to our non-self-gravitating analytic model (*dashed curves*). A typical protoplanetary disk life time of 3 Myr is plotted for comparison. The crossover time is larger for a lower mean molecular weight.

self-gravitating analytic model, described in §3. The analytic model reproduces the general decline in $t_{\rm run}$ with core mass. The numerical model, which includes self-gravity, has a somewhat steeper mass dependence. A modest correction due to self-gravity is unsurprising, and consistent with the above-mentioned trend in $M_{\rm atm}/M_{\rm c}$ ratios. Moreover, in the analytic theory, crucial quantities like $M_{\rm atm}$ and L (both roughly $\propto M_{\rm c}^3$ near crossover) have non-linear dependence on core mass, offering plenty of opportunity for self-gravitational corrections.

The effect of mean molecular weight is also shown in Fig. 6. Lower μ values give longer growth times, and vice-versa. For $\mu = 2.0$, which represents the idealized case of an H_2 atmosphere devoid of Helium, $t_{\rm run}$ increases by factors of $\sim 2-3$. Thus fairly drastic changes in atmospheric composition are required for μ to significantly affect core accretion timescales.

Looking ahead to our discussion of the critical core mass in §5.2, Fig. 6 shows that $t_{\rm run}$ equals a characteristic disk lifetime of 3 Myr for a core mass of $M_{\rm crit} \approx 7\,M_\oplus$ (for the standard case of $\mu = 2.35$).

5.1.2. *Disk Temperature and Pressure*

Fig. 7 shows how the crossover time varies with disk temperature, $T_{\rm d}$, or pressure, $P_{\rm d}$, holding the other quantity fixed. The analytic model roughly reproduces the temperature and pressure scalings, again with some discrepancies due mainly to the neglect of self-gravity. Temperature variations are much more significant than pressure variations (note the difference in logarithmic and linear axes). Since midplane disk conditions depend only on temperature and pressure in our model[5], the dominant effect of disk location is temperature.

The decline in growth times at colder temperatures arises from a variety of competing effects. Briefly, the larger Bondi radius and lower dust opacity at lower temperatures accelerate growth, overpowering the inherently lower cooling luminosity at lower temperatures. Growth times depend only weakly on, but do fall slightly with, pressure. The nearly exponential increase in pressure and density with depth through the radiative zone means that cooling, which is regulated at the RCB, has only a logarithmic dependence on disk pressure. Section 3 explains these effects in more detail.

[5] See Equation (1). When gap opening is considered in models of later growth stages, the orbital frequency and effective viscosity become relevant as well.

5.2. *Critical Core Mass*

The critical core mass declines with distance from the star, as shown in Fig. 8 for our standard disk model. The main reason for the decline, as explained above, is that atmospheres grow faster at colder temperatures. The lower densities and pressures in the outer disk have a much smaller effect. Since the vast majority of disk models have a disk temperature that declines with a, our qualitative result is robust. We also show that higher μ values give lower values of $M_{\rm c,crit}$.

The average power-law decline from 1 to 100 AU (not plotted) is $M_{\rm c,crit} \propto a^{-0.3}$, for both choices of μ. While not a drastic decline, the ability of distant low mass cores to accrete gas efficiently is significant for the interpretation of direct imaging surveys. However our model offers no guarantee of copious giant planets at large distances. Many histories of solid accretion are possible, and solid cores may grow too slowly to allow the rapid gas accretion that we model.

Our non-self-gravitating analytic model (dashed curves in Fig. 8) over-predicts the steepness of the decline in $M_{\rm c,crit}$ vs. a. This discrepancy is not surprising, as we have shown that self-gravity strongly affects evolution, even before runaway growth begins and the crossover mass is reached.

Fig. 9 shows that reducing the opacity by an order of magnitude significantly reduces $M_{\rm c,crit}$. Furthermore, this opacity effect is stronger at larger distances. The opacity reduction by a factor of 10 lowers $M_{\rm c,crit}$ at 5 AU by a factor of ~ 2.5 and at 100 AU by a factor of ~ 3.5. Atmospheric opacity is a dominant uncertainty in core accretion modelling. However, unless atmospheric opacity varies significantly with disk radius, the general decline in $M_{\rm c,crit}$ vs. a should hold. For our scenario of negligible ongoing planetesimal accretion, it is tempting to think that dust could settle out of the radiative zone, lowering the opacity (Podolak 2003). However, since opacity near the RCB is a crucial factor, we speculate that convective overshoot may prevent very low opacities.

6. NEGLECTED EFFECTS

6.1. *Hydrodynamic Effects*

The neglect of hydrodynamical effects in our model is best discussed in terms of the thermal mass, $M_{\rm th}$, and the lengthscales introduced in §2.2. In the low mass regime, $M_{\rm p} < M_{\rm th}/\sqrt{3}$, where $R_{\rm B} < R_{\rm H}$ we assume that hydrostatic balance holds out to the outer boundary at $R_{\rm H}$. In this low mass regime, Ormel (2013) calculated the flow patterns driven by stellar tides and disk headwinds. On scales $\gtrsim R_{\rm B}$ the flows no longer circulate the planet: they belong to the disk. Nevertheless, the density structure outside $R_{\rm B}$ remains spherically symmetric and hy-

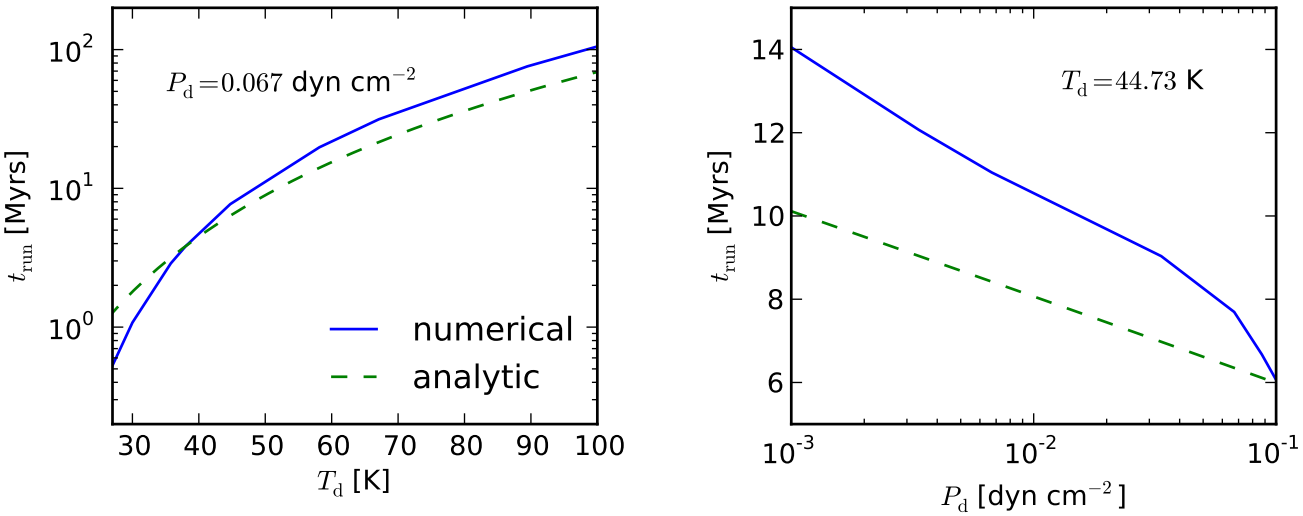

FIG. 7.— Crossover time as a function of disk temperature (*left*) and pressure (*right*) around a $M_c = 5M_\oplus$ core. The disk pressure or temperature (*left* or *right*, respectively) are fixed at values for 10 AU in our disk model. The analytic scalings are plotted for comparison, as described in the text. Gas accretion slows down significantly at higher temperatures, but only speeds up modestly as the disk pressure or density increase.

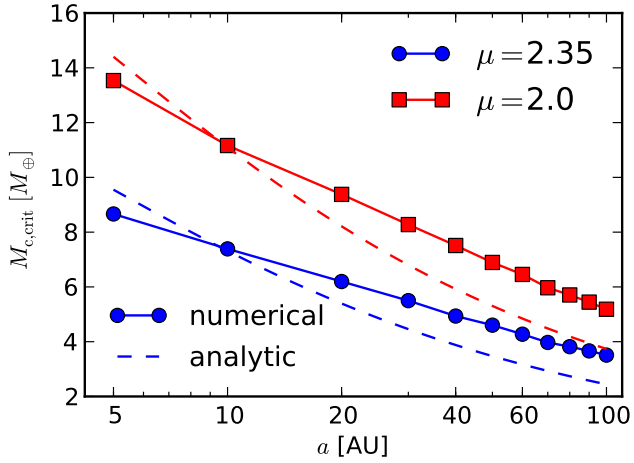

FIG. 8.— The critical core mass as a function of semi-major axis, for a disk lifetime 3 Myrs and two values of the mean molecular weight ($\mu = 2.35$ is standard). The decline in $M_{c,crit}$ with distance is a robust result for standard disk models. The analytic model, which neglects self-gravity, over-predicts the steepness of the decline.

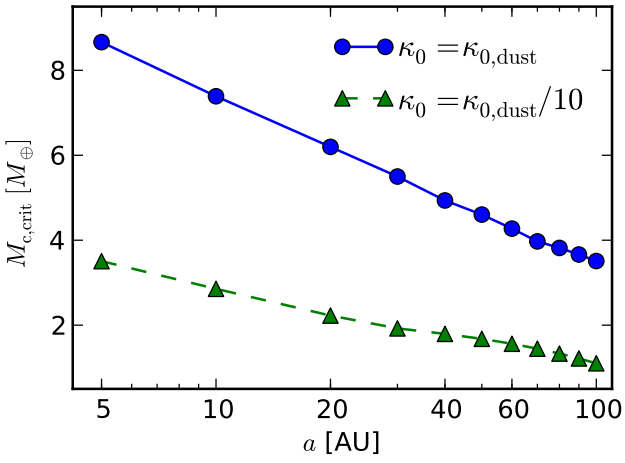

FIG. 9.— Critical core masses vs. distance for standard and reduced (by a factor of ten) dust opacities. Lower opacities give significantly lower $M_{c,crit}$ values. Atmospheric opacity remains a large uncertainty in core accretion models.

drostatic. Even if these flows do not destroy hydrostatic balance, they could affect the planet's cooling. We expect such effects to be weak, as heat losses at greater depths dominate planetary cooling, but more study is needed.

At higher masses, non-hydrostatic effects become more severe. At $M_p \gtrsim M_{th}$ planets can open significant gaps (Zhu et al. 2013). At yet higher masses accretion instabilities could occur (Ayliffe & Bate 2012). However in this high mass regime we already know that the spherically symmetric approximation breaks down, as does our approximate cooling model (*discuss elsewhere and cite*).

Thus by restricting our attention to low masses, neglected hydrodynamic effects should be minor. Moreover since $M_{th} \propto a^{6/7}$ increases with disk radius, spherical hydrostratic models like ours have a greater range of applicability in the outer regions of disks.

6.2. *Realistic Opacities and EOS*

some comments on sublimation and radiative windows here (current text rough). upshot is the outer disk is good.

Real dust opacities exhibit a more complicated behavior that depends on grain composition. Opacities drop by order unity when ice grains sublimate for $T \gtrsim 150$ K and they drop by orders of magnitude when silicate grains evaporate above $T \gtrsim 1500$ K (Semenov et al. 2003; Ferguson et al. 2005). While protoplanetary atmospheres get significantly hotter than 1500 K, our model depends on opacity only in the upper radiative zones, which are cool enough to remain dusty. For our opacity approximations to be valid, we must restrict our model to the lower temperatures of the outer disk.

A second radiative zone inside the convection zone, a "radiative window," is possible. Dust sublimation at shallow depths – giving a low κ and P in Equation (11) – could cause such a window. Our two layer model ignores such complications.

7. CONCLUSIONS

REFERENCES

Arras, P., & Bildsten, L. 2006, ApJ, 650, 394
Ayliffe, B. A., & Bate, M. R. 2012, MNRAS, 427, 2597
Bell, K. R., & Lin, D. N. C. 1994, ApJ, 427, 987
Chiang, E., & Youdin, A. N. 2010, Annual Review of Earth and Planetary Sciences, 38, 493
Ferguson, J. W., Alexander, D. R., Allard, F., Barman, T., Bodnarik, J. G., Hauschildt, P. H., Heffner-Wong, A., & Tamanai, A. 2005, ApJ, 623, 585
Fortney, J. J., Marley, M. S., & Barnes, J. W. 2007, ApJ, 659, 1661
Hubickyj, O., Bodenheimer, P., & Lissauer, J. J. 2005, Icarus, 179, 415
Kippenhahn, R., & Weigert, A. 1990, Stellar Structure and Evolution
Marleau, G.-D., & Cumming, A. 2013, arXiv:1302.1517
Ormel, C. W. 2013, MNRAS, 428, 3526
Podolak, M. 2003, Icarus, 165, 428
Pollack, J. B., Hubickyj, O., Bodenheimer, P., Lissauer, J. J., Podolak, M., & Greenzweig, Y. 1996, Icarus, 124, 62
Semenov, D., Henning, T., Helling, C., Ilgner, M., & Sedlmayr, E. 2003, A&A, 410, 611
Youdin, A. N., & Mitchell, J. L. 2010, ApJ, 721, 1113
Zhu, Z., Stone, J. M., & Rafikov, R. R. 2013, ApJ, 768, 143

APPENDIX

A. DERIVATION OF THE GLOBAL ENERGY EQUATION

To derive the global energy equation (16) for an embedded protoplanets, we generalize the analogous calculations in stellar structure theory, e.g. in §4.3 of Kippenhahn & Weigert (1990). For our problem we add the effects of finite core radius, surface pressure and mass accretion.We start with the local energy equation (10d) whose more natural form in Lagrangian (mass) coordinates is $\partial L/\partial m = \epsilon - T\partial S/\partial t$. Integrating from the core to a higher shell with enclosed mass M gives:

$$L - L_{\rm c} = \int_{M_{\rm c}}^{M} \frac{\partial L}{\partial m} dm \tag{A1a}$$

$$= \int_{M_{\rm c}}^{M} \left(\epsilon - T\frac{\partial S}{\partial t}\right) dm \tag{A1b}$$

$$= \Gamma - \int_{M_{\rm c}}^{M} \frac{\partial u}{\partial t} dm + \int_{M_{\rm c}}^{M} \frac{P}{\rho^2}\frac{\partial \rho}{\partial t} dm\,. \tag{A1c}$$

with $\Gamma = \int \epsilon dm$ the integral of the direct heating rate and applying the law of thermodynamics in the final step.

The global energy equation is derived by eliminating the partial time derivatives in Equation (A1c), which are performed at a fixed mass, in favor of total time derivatives, denoted with overdots. For instance the surface radius, R, evolves as

$$\dot{R} = \frac{\partial R}{\partial t} + \frac{\dot{M}}{4\pi R^2 \rho_M} \tag{A2}$$

where $\partial R/\partial t$ gives the Lagrangian contraction of the "original" shell, and mass accretion through the upper boundary at rate $\dot{M}$ also changes the shell location. Similarly the volume, $V = (4\pi/3)r^3$, and pressure at the outer shell evolve as

$$\dot{V}_M = \frac{\partial V_{\rm M}}{\partial t} + \frac{\dot{M}}{\rho_{\rm M}} \tag{A3a}$$

$$\dot{P}_M = \frac{\partial P_{\rm M}}{\partial t} + \frac{\partial P_M}{\partial m}\dot{M} = \frac{\partial P_{\rm M}}{\partial t} - \frac{GM}{4\pi R^4}\dot{M}\,. \tag{A3b}$$

This derivation holds the core mass and radius fixed, $\dot{M}_{\rm c} = \dot{R}_{\rm c} = 0$. Therefore the core pressure satisfies

$$\dot{P}_{\rm c} = \partial P_{\rm c}/\partial t\,. \tag{A4}$$

The internal energy integral follows simply from Leibniz's rule as

$$\int_{M_{\rm c}}^{M(t)} \frac{\partial u}{\partial t} dm = \dot{U} - \dot{M} u_M\,. \tag{A5}$$

To make further progress we require the virial theorem:

$$E_G = -3\int_{M_{\rm c}}^{M} \frac{P}{\rho} dm + 4\pi(R^3 P_M - R_{\rm c}^3 P_{\rm c}) \tag{A6}$$

which follows from Equations (10a), (10b) and (14) by integrating hydrostatic balance in Lagrangian coordinates. As an aside, the integral in equation (A6) can be evaluated for a polytropic EOS to give simple expressions for the total energy:

$$E = (1-\zeta)U + 4\pi(R^3 P_M - R_c^3 P_c) \tag{A7a}$$

$$= \frac{\zeta-1}{\zeta} E_G + \frac{4\pi}{\zeta}(R^3 P_M - R_c^3 P_c) \tag{A7b}$$

where $\zeta \equiv 3(\gamma - 1)$. We will not make this assumption and will keep the EOS general.

To express the work integral, the final term in Equation (A1c), in terms of changes to gravitational energy we first take the time derivative of Equation (A6):

$$\dot{E}_G = 3\int_{M_c}^{M} \frac{P}{\rho^2}\frac{\partial \rho}{\partial t} dm - 3\int_{M_c}^{M} \frac{\partial P}{\partial t}\frac{dm}{\rho} - 3\frac{P_M}{\rho_M}\dot{M} + 3\dot{P}_M V_M - 3\dot{P}_c V_c + 3P_M \dot{V}_M \,. \tag{A8}$$

The first integral in Equation (A8) is the one we want, but the next one must be eliminated. The time derivative of Equation (14) (times four) gives

$$4\dot{E}_G = -4\frac{GM\dot{M}}{R} + 4\int_{M_c}^{M} \frac{Gm}{r^2}\frac{\partial r}{\partial t} dm \tag{A9a}$$

$$= -4\frac{GM\dot{M}}{R} + 4\pi\int_{M_c}^{M} r^3 \frac{\partial}{\partial m}\frac{\partial P}{\partial t} dm \tag{A9b}$$

$$= -4\frac{GM\dot{M}}{R} - 3\int_{M_c}^{M} \frac{\partial P}{\partial t}\frac{dm}{\rho} + 3V_M \frac{\partial P_M}{\partial t} - 3V_c \frac{\partial P_c}{\partial t} \tag{A9c}$$

where Equations (A9b) and (A9c) use hydrostatic balance and integration by parts.

Subtracting Equations (A5) and (A9c) and rearranging terms with the help of Equations (A2), (A3) and (A4) gives

$$\int_{M_c}^{M} \frac{P}{\rho^2}\frac{\partial \rho}{\partial t} dm = -\dot{E}_G - \frac{GM\dot{M}}{R} - P_M \frac{\partial V_M}{\partial t} \,. \tag{A10}$$

Combining Equations (A1c), (A5) and (A10), we reproduce Equation (16) with the accreted specific energy $e_M \equiv u_M - GM/R$.

B. ANALYTIC COOLING MODEL DETAILS

TODO (academic): Figure out if theta ¡ 1 is actually required? Should be but need to check